Hybrid 1D Plasmonic/Photonic Crystals for Optical Detection of Bacterial Contaminants

Giuseppe Maria Paternò[1†*], Liliana Moscardi[1,2†], Stefano Donini[1], Davide Ariodanti[3], Ilka Kriegel[4], Maurizio Zani[2], Emilio Parisini[1], Francesco Scotognella[1,2] and Guglielmo Lanzani[1,2*]

[1]Center for Nano Science and Technology@PoliMi, Istituto Italiano di Tecnologia, Via Giovanni Pascoli, 70/3, 20133 Milano, Italy;

[2]Dipartimento di Fisica, Politecnico di Milano, Piazza Leonardo da Vinci 32, 20133 Milano, Italy.

[3]Dipartimento di Chimica, Materiali e Ingegneria Chimica "Giulio Natta", Piazza Leonardo da Vinci 32, 20133 Milano, Italy.

[4]Department of Nanochemistry, Istituto Italiano di Tecnologia (IIT), via Morego, 30, 16163 Genova, Italy

[†]These authors contributed equally to this work

[*] Corresponding authors

Abstract

Photonic crystal-based biosensors hold great promise as valid and low-cost devices for real-time monitoring of a variety of biotargets. Given the high processability and easiness of read-out even for unskilled operators, these systems can be highly appealing for the detection of bacterial contaminants in food and water. Here, we propose a novel hybrid plasmonic/photonic device that is responsive towards *Escherichia coli*, which is one of the most hazardous pathogenic bacterium. Our system consists of a thin layer of silver, a metal that exhibits both a plasmonic behavior and a well-known biocidal activity, on top of a solution processed 1D photonic crystal. We attribute the bio-responsivity to the modification of the dielectric properties of the silver film upon bacterial contamination, an effect that likely stems from the formation of polarization charges at the Ag/bacterium interface within a sort of “bio-doping” mechanism. This, interestingly, triggers a visual red-shift in the photonic crystal color. This work demonstrates that our plasmonic/photonic device can be a low-cost and portable platform for the detection of common contaminants in food and water.

Introduction

The integration of sensing elements with photonic crystals (PhCs) allows a simple readout of the detection event, often based on color changing, fostering applications in portable, and cheap applications.[1–5] For instance, photonic sensing might be of particular interest for the detection of contaminants or pathogenic bacteria in food and water, as in this case the vast majority of the existing detection systems are relatively time and money-consuming mostly due to complexity of the read-out.[6–8]

Briefly, the periodicity in the dielectric constant along 1, 2 or 3 spatial dimensions gives rise to a forbidden gap for photons (stop-band) of specific wavelengths that, in turns, confers structural reflection colors to the material.[9] Focusing on the simplest case of one-dimensional photonic crystals (also known as Bragg stacks, BSs) in which the stop-band arises from the alternation of layers with high/low refractive index, the structural color can be easily tuned by varying either the dielectric contrast or the periodicity of the alternated layers (or both). This can be achieved by the introduction of a medium within the 1D structure, as enabled by porosity at the meso/nanoscale in the BSs.[10–12, 13–17] To further enhance selectivity and to detect large or complex analytes (i.e. bacteria and biomolecules) it is also possible to chemically functionalize the surface of porous BS,[18–20] although such a step would hamper easy scalability of the process. To this end, the fabrication of photonic sensors from scalable and low-cost procedures allowing fast and reliable detection of contaminants (i.e. in food and water) is highly desirable.[21]

In this context, our recent work has been focused on the development of responsive BSs made of alternating layer of dielectric materials and electro-optical responsive plasmonic materials, which are fabricated from easy and low-cost solution-based processes. In particular, the integration of metal plasmonic systems in PhCs provides both high sensitivity to environmental

changes as well peculiar sensing capabilities [22,23] due to the specific metal interactions.[24–26] Carrier density modulation results in the change of the refractive index that ultimately determines the photonic stop-band, thus offering a handle for easy optical detection. We have shown that such peculiar feature of plasmonic materials can be exploited to build-up electro-optical switches based on the photonic reflection shift upon photo-electro doping of indium tin oxide (ITO) nanoparticles (NPs) in SiO_2/ITO and TiO_2/ITO photonic crystals,[27,28] and electro doping of silver NPs in TiO_2/Ag crystals.[29] Furthermore, the specific interactions occurring at the metal surface in contact with the analytes can be exploited for label-free and low-cost (bio)sensing purposes-[30,31] It is well-known that silver films and NPs exhibit antibacterial properties.[32–36] Although the exact antibacterial mechanism is still under debate[37] (see supplementary information section for a brief discussion on Ag bactericidal mechanism), many reports agree that electrostatic attraction is crucial for the Ag adhesion to the bacterial membrane and to the consequent bactericidal activity possibly mediated by transmembrane ion penetration.[36,38–40] Interestingly, this might lead to a modification of Ag charge carriers density and plasmon resonance upon bacteria/Ag interaction, for example as a result of polarization[41] charges accumulating at the bacteria/Ag interface.

Here, we show that a hybrid plasmonic/photonic device consisting of a thin layer of silver deposited on top of a solution processed BS is responsive towards one of the most common bacterial contaminant, namely *Escherichia coli*. Our data suggest that the change in the plasmon charge density likely originates from the formation of polarization charges at the bacterium/Ag interface, resulting in a variation of the plasmon resonance. This eventually determines a change in the photonic read-out (red-shift) that amplifies and translates the plasmonic effect occurring in the UV (380-400 nm) to the more convenient spectral region for (600-530 nm). These promising

results indicate that hybrid plasmonic/photonic PhCs can represent a novel class of low-cost devices responsive towards common contaminants in food and water.

Experimental section

Photonic crystals fabrication. Porous 1D PhCs were fabricated by alternating layers of SiO_2 and TiO_2 via spin-casting deposition from their colloidal aqueous dispersions following the procedure employed in past experiments.[27,28] Firsly, we suspended the TiO_2 (Gentech Nanomaterials, average size 5 nm) and SiO_2 nanoparticles (Sigma Aldrich LUDOX SM-30, average size 8 nm) in MilliQ distilled water to obtain a concentration of 5 wt. %. The dispersions were then sonicated for 2 h at 45 °C (Bandelin SONOREX Digital 10 P) and filtered with a 0.45 μm PVDF filter. The glass substrates were previously cleaned by means of ultra-sonication in isopropanol (10 min) and acetone (10 min), and then subjected to an oxygen plasma treatment (Colibrì Gambetti, 10 min) to increase wettability. During the fabrication of the PhCs, the dispersions were continuously kept in sonication at 45 °C to maintain homogeneity of the dispersions during the whole process. The fabrication of the crystals was performed by alternating the deposition of the two materials through spin-coating (Laurell WS-400-6NNP-Lite) with a speed of 2000 rpm. After each deposition, the samples were annealed on a hot-plate for 20 min at 350 °C. Finally, we deposited a 8 nm thick silver layer on top of the photonic structure (or glass substrate only) via thermal evaporation (MBRAUN metal evaporator).

Bacteria culture. A single colony from *Escherichia coli rosetta* (DE3) strain carrying a pET23a (+) plasmid was inoculated in Lauria Bertani (LB) broth in presence of Ampicillin (50 μg/ml) and incubated overnight at 37ºC with shaking at 200 rpm until stationary phase was reached. Then,

bacterial suspension turbidity (expressed as optical density at 600nm; O.D 600) was diluted to O.D 600 ~ 0.5 in LB broth (no antibiotic). The suspension (500 μL) was spread over the LB agar plate. The Ag/PhCs were placed in the center of Petri dish with top silver layer facing the contaminated surface (or LB only for the control experiment) and incubated 24 h at 37 °C. We also dip the devices in either LB only (control) or LB/*E.coli* mixture to mimic exposure to contaminated liquid samples (0.1, 0.5 and 1.2 O.D.). Same protocol was also repeated for silver thin films on glass substrates, to understand the effect of bacteria exposition on the silver plasmon resonance. Data were averaged over two sets of measurements (six samples per measurement).

Optical characterization. The optical characterization was performed using a spectrophotometer (Perkin Elmer Lambda 1050 WB), measuring both the percentage loss of transmittance and reflectance before, after exposure to *E. coli* and after rinsing with deionized water. To disentangle the photonic from plasmonic contribution to the overall transmission of the sample, we recorded the transmission as a function of the incidence angle, showing a blue-shift of the photonic stop-band upon increase of the angle, in accordance with the Bragg-Snell law.

Scanning electron microscopy. We used a Tescan MIRA3. The measurements were performed at a voltage of 5 kV and backscattered electrons were detected. The sample was covered with carbon paste to improve conductivity

Transfer matrix method. *Refractive indexes of the Ag layers, and the SiO_2 and TiO_2 layers composing the photonic crystal*. We employ the Drude model to describe the plasmonic response.[42] Thus, the frequency dependent complex dielectric function of silver can be written as:

$$\varepsilon_{ITO,\omega} = \varepsilon_{1,\omega} + i\varepsilon_{2,\omega} \quad (1)$$

where

$$\varepsilon_{1,\omega} = \varepsilon_{\infty} - \frac{\omega_P^2}{(\omega^2 - \Gamma^2)} \quad (2)$$

and

$$\varepsilon_{2,\omega} = \frac{\omega_P^2 \Gamma}{\omega(\omega^2 - \Gamma^2)} \quad (3)$$

where ω_P is the plasma frequency and Γ is the free carrier damping. The plasma frequency is $\omega_P = \sqrt{Ne^2/m^*\varepsilon_0}$, with *N* number of charges, *e* the electron charge, m^* the effective mass and ε_0 the vacuum dielectric constant. For silver, we use $N = 5.76 \times 10^{28}\ charges/m^3$, $m^* = 0.96/m_0\ kg$. For the free carrier damping, we use $\Gamma = 0.018$. Finally, the value of the high frequency dielectric constant, $\varepsilon_{\infty} = 4$. The parameters for silver nanoparticles are taken from.[43]

The wavelength dependent refractive index of TiO_2 can be written as:[44]

$$n_{TiO_2}(\lambda) = \left(4.99 + \frac{1}{96.6\lambda^{1.1}} + \frac{1}{4.60\lambda^{1.95}}\right)^{1/2} \quad (4)$$

where λ is the wavelength [in micrometers, and $\varepsilon_{TiO_2}(\lambda) = n^2_{TiO_2}(\lambda)$]. Instead, the wavelength dependent refractive index of SiO_2 can be described by the following Sellmeier equation:[45]

$$n^2_{SiO_2}(\lambda) - 1 = \frac{0.6961663\lambda^2}{\lambda^2 - 0.0684043^2} + \frac{0.4079426\lambda^2}{\lambda^2 - 0.1162414^2} + \frac{0.8974794\lambda^2}{\lambda^2 - 9.896161^2} \quad (5)$$

where λ is the wavelength in micrometers [also for SiO_2 $\varepsilon_{SiO_2}(\lambda) = n^2_{SiO_2}(\lambda)$].

Taking into account the infiltration of LB in the silver layer and in the silica and titania layers of the photonic crystal, we determine the effective dielectric function of the SiO_2:air layer (we call it $\varepsilon_{eff2,\omega}$) by using the Maxwell-Garnett effective medium approximation:[46,47]

$$\varepsilon_{eff,\omega} = \varepsilon_{LB} \frac{2(1-f)\varepsilon_{LB}+(1+2f)\varepsilon_{\omega}}{2(2+f)\varepsilon_{LB}+(1-f)\varepsilon_{\omega}} \quad (6)$$

where f is the filling factor of the silver, SiO_2, or TiO_2 layers and ε_{ω} is the dielectric function of the silver, SiO_2, or TiO_2 layers. In this study we choose $f_{Ag} = 0.5$; $f_{SiO_2} = 0.6$; $f_{TiO_2} = 0.6$. The dielectric constant in the visible range for LB is approximated to the one of water, thus $\varepsilon_{LB} = 1.769$.

Transmission of the multilayer photonic crystal: We use the three effective refractive indexes of the Ag:LB, SiO_2:LB, TiO_2:LB layers to study the light transmission through the photonic structure by employ the transfer matrix method.[48,49] For a transverse electric (TE) wave the transfer matrix for the *k*th layer is given by

$$M_k = \begin{bmatrix} cos\left(\frac{2\pi}{\lambda} n_k d_k\right) & -\frac{i}{n_k} sin\left(\frac{2\pi}{\lambda} n_k d_k\right) \\ -in_k sin\left(\frac{2\pi}{\lambda} n_k d_k\right) & cos\left(\frac{2\pi}{\lambda} n_k d_k\right) \end{bmatrix} \quad (7)$$

with n_k the refractive index and d_k the thickness of the layer. In this study the thickness of the Ag:LB layers is 8 nm, while the thickness of the SiO_2:LB layers and TiO_2:LB layers is 100 nm.

The product $M = M_1 \cdot M_2 \cdot \ldots \cdot M_k \cdot \ldots \cdot M_s = \begin{bmatrix} m_{11} & m_{12} \\ m_{21} & m_{22} \end{bmatrix}$ gives the matrix of the multilayer (of *s* layers). The transmission coefficient is

$$t = \frac{2n_s}{(m_{11}+m_{12}n_0)n_s+(m_{21}+m_{22}n_0)} \quad (8)$$

with n_s the refractive index of the substrate (in this study $n_s = 1.46$) and n_0 the refractive index of air. Thus, the light transmission of the multilayer photonic crystal is

$$T = \frac{n_0}{n_s}|t|^2 \quad (9)$$

Results and discussion

The multilayered 1D photonic structures show the expected structural color in reflection (5 × SiO_2/TiO_2 bilayers) as shown in **Figure 1a-b,** while electron microscopy images are reported in **Figure S1a.** The BSs were fabricated via simple spin-coating deposition of the respective aqueous colloidal dispersions. This is a key point in the view to scale the process by means of large-area and low-cost deposition techniques, such as ink-jet printing and roll-to-roll. On top of the dielectric BS we deposited a thin layer of silver (8 nm, **Figure S1b** for the electron microscopy image), to exploit both the plasmonic behaviour and the marked and well-documented biocidal properties. The thin silver layer is in-fact a defective cap layer of the photonic crystal that affect the optical response of the BS through the silver free carrier density (Drude model).[50] Therefore, the main idea here is to exploit the possible change in the silver complex dielectric function driven by Ag/bacteria interaction, to modify the dielectric properties at the BS/metal interface and, thus, the BS optical read-out. With this in mind, we selected the minimum Ag thickness achievable with our deposition apparatus, to localize strongly the plasmonic response at the close proximity of the BS interface. To observe both the plasmonic and photonic contributions to the overall sample transmission and disentangle them, we carried out measurements as a function of incidence angle (**Figure 1c**). These data show a blue shift of the photonic band-gap (586 nm at 0°) by increasing

the angle in agreement with the Bragg-Snell law (inset **Figure 1c**),[22] while the plasmonic peak at 500 nm does not display any angular dependence.

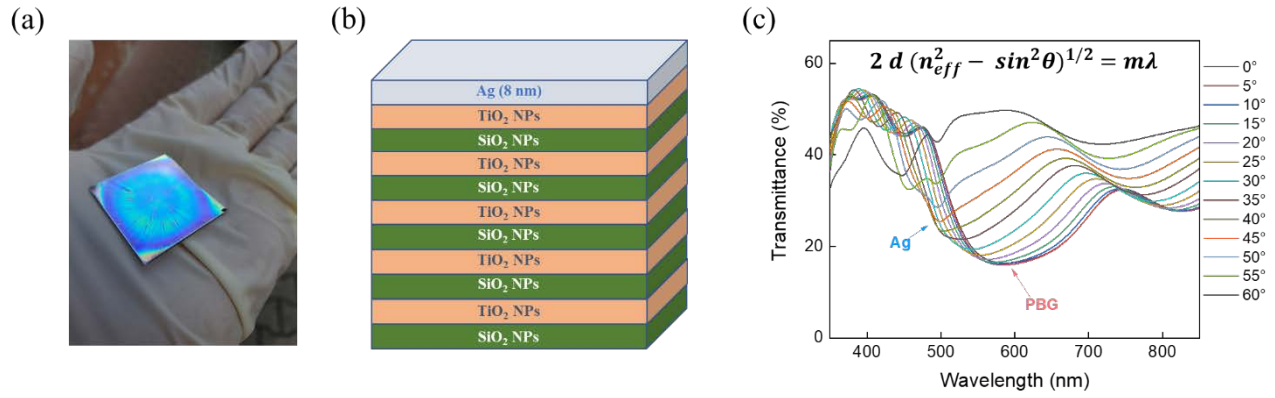

Figure 1. (a) Picture of the fabricated 1D photonic crystal with a silver capping layer and (b) sketch of the multilayered structure. (c) Light transmission of the Ag/$(SiO_2/TiO_2)_5$ photonic crystals as a function of the light incidence angle (inset Bragg-Snell equation).

To evaluate the effect of bacteria on the optical properties of silver, we first exposed Ag films to LB only (control experiment, **Figure 2a**) and then to *E. coli* (**Figure 2b**) in agar plate, as described in the experimental section. We observe that the sample exposed to LB undergoes a substantial red-shift (60 nm) that is likely due to the infiltration of the aqueous culture medium across the silver grains, leading to an increase in the effective refractive index[51]. On the other hand, there are two main effects upon contamination of the silver layer with *E. coli* in LB medium, namely: i. a blue shift at peak maximum (30 nm) with respect to LB only contamination; ii. a clear increase of the plasmonic absorption at the high energy side (330 - 400 nm). We interpret the reduced bathochromic shift upon adding *E. coli* + LB as due to a blue-shift in the plasmon resonance that counterbalances the red-shift induced by LB alone. Such blue-shift in the plasmon resonance could stem from the formation of polarization charges at the silver-bacterium interface leading to an increase of the charge carrier density. [27,29] Furthermore, to mimic exposure to

contaminated liquids, we dip our samples in LB medium (control) or in LB/*E. coli* mixture with increasing bacterial loading (0.1, 0.5 and 1.2 O.D.) and measured their plasmonic response (**Figure S2**). We essentially observed an analogous effect, with a read-shift attenuation at peak maximum (60 nm for LB only, 50 nm for 0.1 O.D., 40 nm for 0.5 O.D. and 1.2 O.D.), as well as an enhanced absorption at the high energy side as a function of bacterial loading.

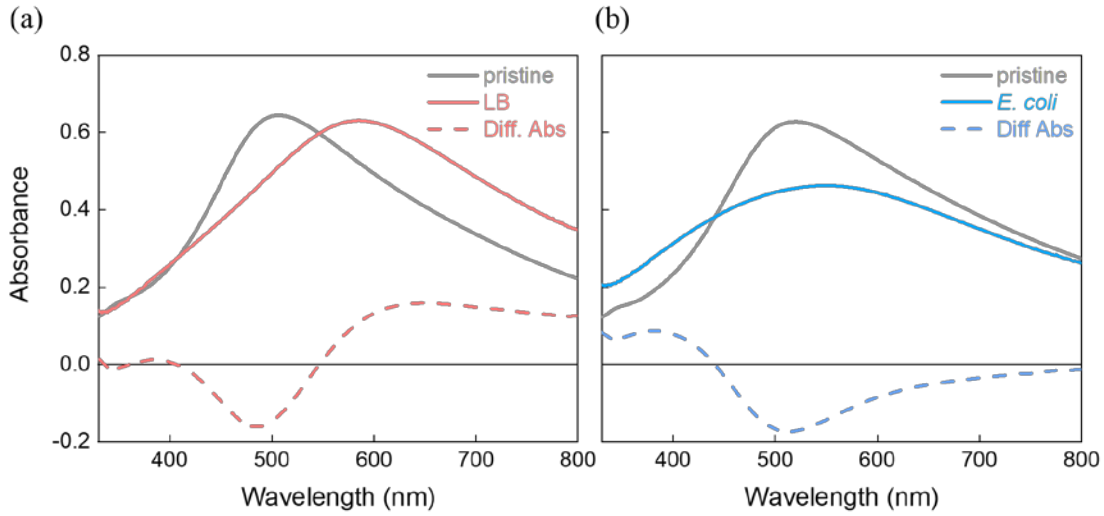

Figure 2. (a) Optical absorption of a Ag thin film (8 nm on glass) before (grey line) and after (red line) exposure to LB on agar plate and (b) to LB/*E. coli* (red line). Dotted lines show the differential absorption (absorbance after – absorbance before exposure) and highlight the different Ag plasmonic response when exposed to either the control or to bacterial medium.

After having investigated the Ag plasmonic response of metallic film alone upon contamination with *E. coli*, we proceed to study how this is affecting the all optical read-out in presence of the photonic crystal (**Figure 3**). Qualitatively both exposure to LB or *E. coli* + LB leads to the same behavior, namely enhanced reflectivity, resonance broadening (20 nm) and read-shift of the stop-band. Again we have two physical phenomena concurring to these changes: i) infiltration of LB inside the porous BS architecture, leading to enhanced effective refractive index (**Figure 3a-b**), and ii) the modulation of the plasmon resonance in the top metal layer. The

magnitude of the reflectivity read-shift however is much larger in presence of *E. coli* in LB, featuring max. shift of 30 nm (average 26 nm) compared to LB alone with +5 nm. Interestingly, this translates into a modification of the structural color upon bacterial contamination that can be detected by eye, while LB alone does not cause any appreciable visual shift (**Figure 3d**). Such an easy color read-out is an asset for the development of low-cost devices for the detection of bacterial contaminants. The presence of a well-defined zone of inhibition matching the shape of our samples in conformal contact with the agar medium inoculated with *E. coli* confirms the anti-bacterial activity of our Ag layer (**Figure S3**). Furthermore, this effect seems to be confined within the sample area, suggesting that silver does not appreciably detach from the surface and diffuse in all the agar plate as it happens for silver NPs,[52] a fact that can be of importance for possible applications of these devices in food packaging.[53] To study the optical response of Ag/PhCs in contact with liquid specimens, we also immersed our samples in LB medium or *E. coli*/LB (10 minutes) and measured the transmission (**Figure S4**). Again, we observe a more substantial red-shift for the contaminated samples when compared to the LB case, an effect that scales with bacterial loading (10 nm for LB only, 20 nm for 0.1 O.D. and 0.5 O.D. and 30 nm for 1.2 O.D.). In addition, as a control experiment, we repeated the same experimental procedure on identical 1D photonic crystals but without the top Ag layer, in order to further prove the role of the plasmonic material in the bio-responsivity of our device (**Figure S5**). Here, we could not discriminate any difference between the samples exposed to LB or to LB/*E. coli*, with the exception of the usual 5 nm read-shift and broadening of the stop-band that are connected to liquid condensation and infiltration throughout the porous structure. This confirms that the upper plasmonic layer represents the responsivity element of our hybrid plasmonic/photonic device, as the modification

of the dielectric properties at the Ag/BS interface, which in turns is brought about by Ag/bacteria interaction, governs the total optical read-out.

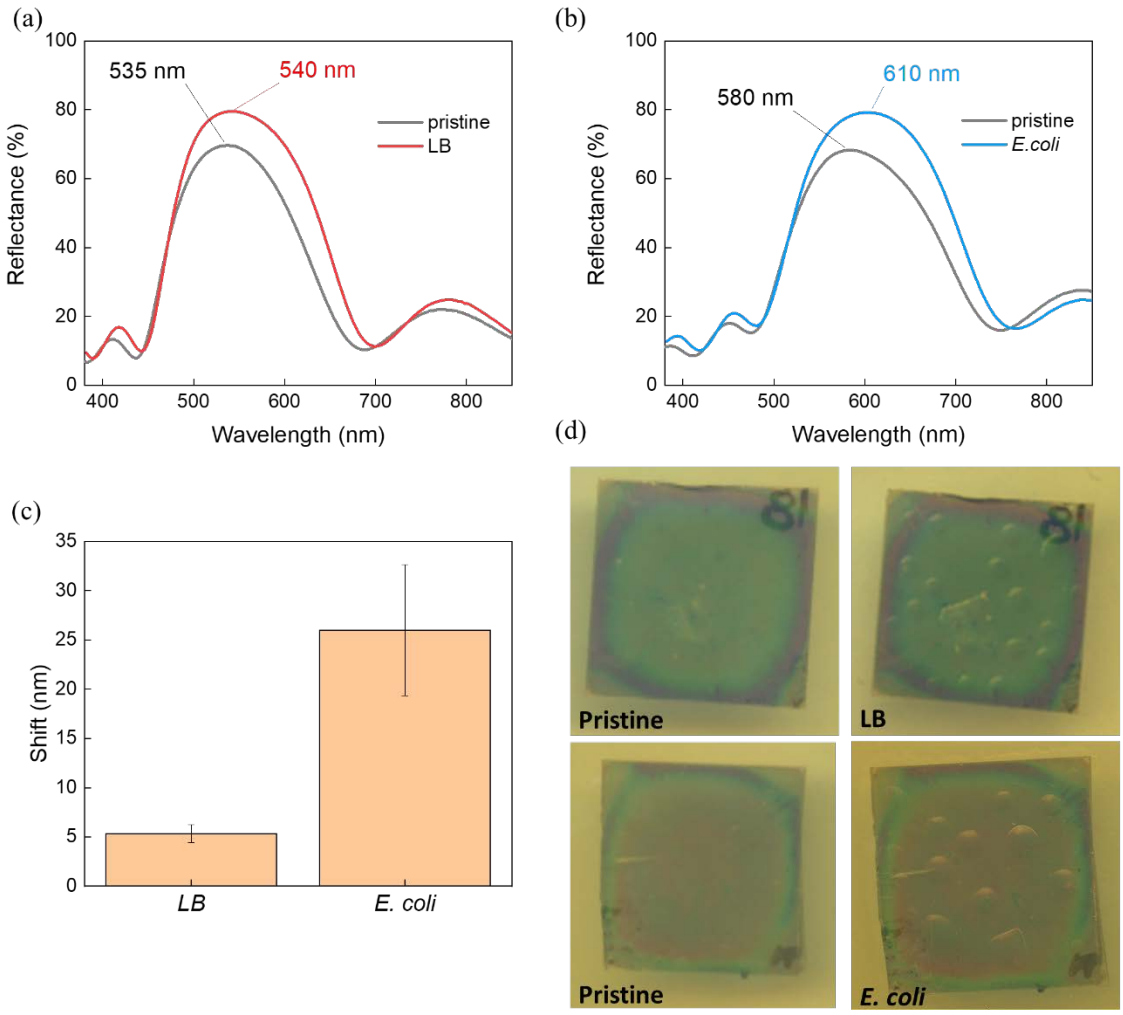

Figure 3. (a) Reflectance spectrum of Ag/1D PhC after exposure to the LB medium (red-line) and (b) *E. coli* (blue-line). (c) Average shift at the stop-band maximum for the LB and *E. coli* contaminated PhCs. Data were averaged over two sets of measurement (six samples per measurement). (d) PhCs reflection color after exposure to LB (no appreciable visual shift) and *E. coli* (red-shift). Bubbles that can be seen on the BS surface are due to air inclusions at the BS–agar interface.

Finally, to obtain insights into the mechanism underpinning the photonic shift, we simulated the transmission spectra as a function of the silver carrier density (**Figure 4a**). For this, we combined the transfer matrix method to model the alternating refractive index of the periodic

structure, with the Maxwell-Garnett effective medium approximation for the description of the effective refractive indexes of the SiO_2/TiO_2 layers soaked with LB (see experimental section), In addition, we made use of the Drude model to account for the plasmonic contribution to the overall dielectric response of the device. We then proceeded to the simulation of the transmission spectra for two different silver charge carrier densities ($n = 5.76 \times 10^{28}\ m^3$ and $6.76 \times 10^{28}\ m^3$) in the LB infiltrated photonic structure, to assess whether the formation of polarization charges at the Ag/bacteria interface (as depicted in **Figure 4b**) would translate into a photonic effect. Indeed, an increased carrier density possibly due to such polarization charges induces a large blue-shift of the plasmon resonance (35 nm) as predicted by the Drude model, while the stop-band exhibits a less obvious 5 nm red-shift. Notably, such a behavior corroborates our experimental data, at least from the qualitative point of view. Note that our model predicts a relatively small stop-band red-shift (5 nm) against a quite substantial plasmonic blue-shift (35 nm), while our experimental data show a large stop-band shift (30 nm) that amplifies a small change in the plasmon resonance upon bacterial contamination. Such a discrepancy can be probably attributed to the kicking in of a different effect that intensifies the dielectric mechanism, for instance a strong field enhancement and confinement at the metal/dielectric interface (i.e. Tamm optical modes).[54,55]

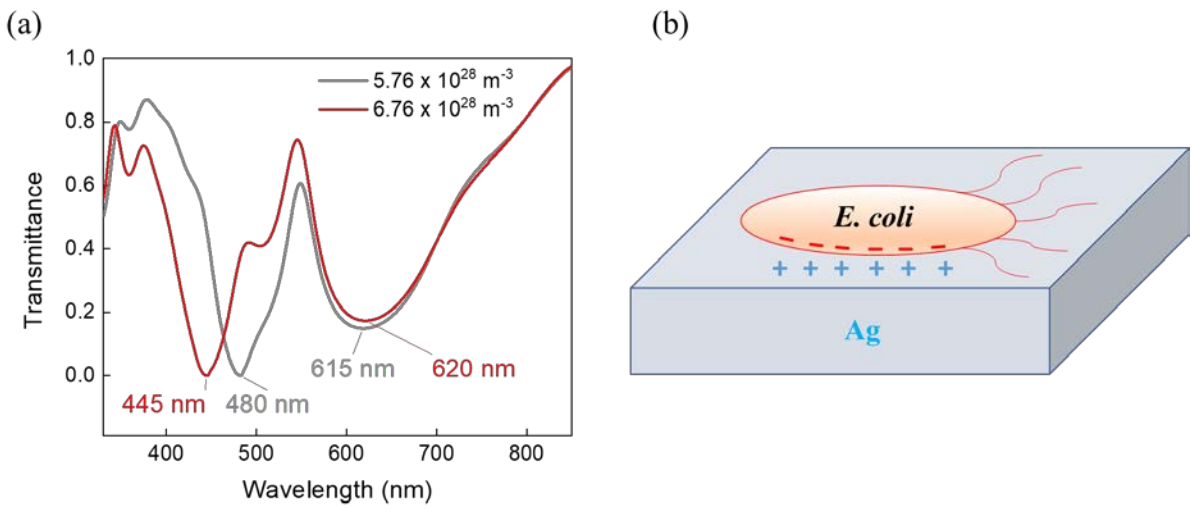

Figure 4. (a) Calculated transmission of the hybrid Ag/BS device for two charge carrier densities. (b) Pictorial representation of the hypothesized mechanism giving rise to both the plasmonic blue-shift (polarization accumulation charge) and stop-band red-shift (increase dielectric contrast at the metal/dielectric interface).

Conclusions

To summarize, we have shown that a hybrid plasmonic/photonic device consisting of a thin layer (8 nm) of the plasmonic and biocidal silver on top of a 1D photonic crystal can be responsive against one of the most hazardous bacterial contaminant in food and water, *Escherichia coli*. Our data points towards a scenario in which the polarization charge at the Ag/bacterium interface causes an increase of the metal charge carrier density that leads to a plasmon blue-shift, within a sort of "bio-doping" mechanism. This, in turns, leads to an increase of the dielectric contrast at the upper interface and a visual red-shift of photonic stop-band. It is worth adding that the photonic band-gap can be placed in any spectral region by a judicious choice of the layer thicknesses, allowing one to translate the photonic read-out in the most convenient part of the spectrum. This, taken together with the quick processability from solution and easiness of the read-out, makes these devices promising for low-cost and real-time monitoring of contaminants in food and water.

Associated content

Supporting information

The Supporting Information is available free of charge on the ACS Publications website.

Discussion on the biocidal activity of silver; scanning electron microscopy images of the silver film and cross-section of the 1D photonic crystal; UV-Vis absorption spectra of the silver films after dipping in liquid LB and *E. coli*/LB mixture; zone of inhibition in the agar plate inoculated with *E. coli*; UV-Vis transmission spectra of the Ag/BSs samples after dipping in liquid LB and *E. coli*/LB mixture; UV-Vis transmission spectra of the BSs without the silver layer before and after exposure to LB or to LB/*E. coli*.

Author information

Corresponding authors

E-mail: Giuseppe.Paterno@iit.it ; Guglielmo.Lanzani@iit.it

Authors contribution

G.M.P., L.M., S.D. and D.A. carried out the experiments. G.M.P. wrote the manuscript, together with L.M., S.D., G.L. and F.S. I.K., M.Z. and F.S. run the simulations. E.M supervised the microbiology work. G.M.P., G.L. and F.S. conceived the work. G.M.P and L.M. contributed equally to this work.

Notes

The authors declare no competing financial interest.

Acknowledgements

References

(1) Ge, J.; Yin, Y. Responsive Photonic Crystals. *Angew. Chemie Int. Ed.* **2011**, *50* (7), 1492–1522. https://doi.org/10.1002/anie.200907091.

(2) Nucara, L.; Greco, F.; Mattoli, V. Electrically Responsive Photonic Crystals: A Review. *J. Mater. Chem. C* **2015**, *3* (33), 8449–8467. https://doi.org/10.1039/c5tc00773a.

(3) Inan, H.; Poyraz, M.; Inci, F.; Lifson, M. A.; Baday, M.; Cunningham, B. T.; Demirci, U. Photonic Crystals: Emerging Biosensors and Their Promise for Point-of-Care Applications. *Chem. Soc. Rev.* **2017**, *46* (2), 366–388. https://doi.org/10.1039/C6CS00206D.

(4) Fenzl, C.; Hirsch, T.; Wolfbeis, O. S. Photonic Crystals for Chemical Sensing and Biosensing. *Angew. Chemie - Int. Ed.* **2014**, *53* (13), 3318–3335. https://doi.org/10.1002/anie.201307828.

(5) Wang, H.; Zhang, K. Q. Photonic Crystal Structures with Tunable Structure Color as Colorimetric Sensors. *Sensors (Switzerland)*. 2013, pp 4192–4213. https://doi.org/10.3390/s130404192.

(6) Meulebroeck; Thienpont; Ottevaere. Photonics Enhanced Sensors for Food Monitoring: Part 1. *IEEE Instrum. Meas. Mag.* **2016**, *19* (6), 35–45. https://doi.org/10.1109/MIM.2016.7777651.

(7) Meulebroeck, W.; Thienpont, H.; Ottevaere, H. Photonics Enhanced Sensors for Food Monitoring: Part 2. *IEEE Instrum. Meas. Mag.* **2017**, *20* (1), 31–37. https://doi.org/10.1109/MIM.2017.7864547.

(8) Meulebroeck, W.; Thienpont, H.; Ottevaere, H. Photonics Enhanced Sensors for Food Monitoring: Part 3. *IEEE Instrum. Meas. Mag.* **2017**, *20* (5), 46–55. https://doi.org/10.1109/MIM.2017.8036698.

(9) Yablonovitch, E. Inhibited Spontaneous Emission in Solid-State Physics and Electronics. *Phys. Rev. Lett.* **1987**, *58* (20), 2059–2062. https://doi.org/10.1103/PhysRevLett.58.2059.

(10) Robbiano, V.; Paternò, G. M.; La Mattina, A. A.; Motti, S. G.; Lanzani, G.; Scotognella, F.; Barillaro, G. Room-Temperature Low-Threshold Lasing from Monolithically Integrated Nanostructured Porous Silicon Hybrid Microcavities. *ACS Nano* **2018**, *12* (5), 4536–4544. https://doi.org/10.1021/acsnano.8b00875.

(11) Bonifacio, L. D.; Lotsch, B. V.; Puzzo, D. P.; Scotognella, F.; Ozin, G. A. Stacking the Nanochemistry Deck: Structural And Compositional Diversity in One-Dimensional Photonic Crystals. *Adv. Mater.* **2009**, *21* (16), 1641–1646. https://doi.org/10.1002/adma.200802348.

(12) Passoni, L.; Criante, L.; Fumagalli, F.; Scotognella, F.; Lanzani, G.; Di Fonzo, F. Self-Assembled Hierarchical Nanostructures for High-Efficiency Porous Photonic Crystals. *ACS Nano* **2014**, *8* (12), 12167–12174. https://doi.org/10.1021/nn5037202.

(13) Orosco, M. M.; Pacholski, C.; Sailor, M. J. Real-Time Monitoring of Enzyme Activity in a Mesoporous Silicon Double Layer. *Nat. Nanotechnol.* **2009**, *4* (4), 255–258. https://doi.org/10.1038/nnano.2009.11.

(14) Colodrero, S.; Ocaña, M.; Míguez, H. Nanoparticle-Based One-Dimensional Photonic Crystals. *Langmuir* **2008**, *24* (9), 4430–4434. https://doi.org/10.1021/la703987r.

(15) Lova, P.; Manfredi, G.; Comoretto, D. Advances in Functional Solution Processed Planar 1D Photonic Crystals. *Adv. Opt. Mater.* **2018**, *6* (24), 1800730. https://doi.org/10.1002/adom.201800730.

(16) Choi, S. Y.; Mamak, M.; von Freymann, G.; Chopra, N.; Ozin, G. A. Mesoporous Bragg Stack Color Tunable Sensors. *Nano Lett.* **2006**, *6* (11), 2456–2461. https://doi.org/10.1021/nl061580m.

(17) Fuertes, M. C.; López-Alcaraz, F. J.; Marchi, M. C.; Troiani, H. E.; Luca, V.; Míguez, H.; Soler-Illia, G. J. A. A. Photonic Crystals from Ordered Mesoporous Thin-Film Functional Building Blocks. *Adv. Funct. Mater.* **2007**, *17* (8), 1247–1254. https://doi.org/10.1002/adfm.200601190.

(18) Chan, S.; Horner, S. R.; Fauchet, P. M.; Miller, B. L. Identification of Gram Negative Bacteria Using Nanoscale Silicon Microcavities [1]. *J. Am. Chem. Soc.* **2001**, *123* (47), 11797–11798. https://doi.org/10.1021/ja016555r.

(19) Bonifacio, L. D.; Puzzo, D. P.; Breslav, S.; Willey, B. M.; McGeer, A.; Ozin, G. A. Towards the Photonic Nose: A Novel Platform for Molecule and Bacteria Identification. *Adv. Mater.* **2010**, *22* (12), 1351–1354. https://doi.org/10.1002/adma.200902763.

(20) Bonifacio, L. D.; Ozin, G. A.; Arsenault, A. C. Photonic Nose-Sensor Platform for Water and Food Quality Control. *Small* **2011**, *7* (22), 3153–3157. https://doi.org/10.1002/smll.201101074.

(21) Adley, C. Past, Present and Future of Sensors in Food Production. *Foods* **2014**, *3* (3), 491–510. https://doi.org/10.3390/foods3030491.

(22) Morandi, V.; Marabelli, F.; Amendola, V.; Meneghetti, M.; Comoretto, D. Colloidal Photonic Crystals Doped with Gold Nanoparticles: Spectroscopy and Optical Switching Properties. *Adv. Funct. Mater.* **2007**, *17* (15), 2779–2786. https://doi.org/10.1002/adfm.200600764.

(23) Robbiano, V.; Giordano, M.; Martella, C.; Stasio, F. Di; Chiappe, D.; De Mongeot, F. B.; Comoretto, D. Hybrid Plasmonic-Photonic Nanostructures: Gold Nanocrescents Over Opals. *Adv. Opt. Mater.* **2013**, *1* (5), 389–396. https://doi.org/10.1002/adom.201200060.

(24) Luther, J. M.; Jain, P. K.; Ewers, T.; Alivisatos, A. P. Localized Surface Plasmon Resonances Arising from Free Carriers in Doped Quantum Dots. *Nat. Mater.* **2011**, *10* (5), 361–366. https://doi.org/10.1038/nmat3004.

(25) Dorfs, D.; Härtling, T.; Miszta, K.; Bigall, N. C.; Kim, M. R.; Genovese, A.; Falqui, A.; Povia, M.; Manna, L. Reversible Tunability of the Near-Infrared Valence Band Plasmon Resonance in Cu2- XSe Nanocrystals. *J. Am. Chem. Soc.* **2011**. https://doi.org/10.1021/ja2016284.

(26) Scotognella, F.; Della Valle, G.; Srimath Kandada, A. R.; Dorfs, D.; Zavelani-Rossi, M.; Conforti, M.; Miszta, K.; Comin, A.; Korobchevskaya, K.; Lanzani, G.; et al. Plasmon Dynamics in Colloidal Cu2-XSe Nanocrystals. *Nano Lett.* **2011**, *11* (11), 4711–4717. https://doi.org/10.1021/nl202390s.

(27) Paternò, G. M.; Iseppon, C.; D'Altri, A.; Fasanotti, C.; Merati, G.; Randi, M.; Desii, A.; Pogna, E. A. A.; Viola, D.; Cerullo, G.; et al. Solution Processable and Optically Switchable 1D Photonic Structures. *Sci. Rep.* **2018**, *8* (1), 3517. https://doi.org/10.1038/s41598-018-21824-w.

(28) Paternò, G. M.; Moscardi, L.; Kriegel, I.; Scotognella, F.; Lanzani, G. Electro-Optic and Magneto-Optic Photonic Devices Based on Multilayer Photonic Structures. *J. Photonics Energy* **2018**, *8* (03), 1. https://doi.org/10.1117/1.JPE.8.032201.

(29) Aluicio-Sarduy, E.; Callegari, S.; del Valle, D. G. F.; Desii, A.; Kriegel, I.; Scotognella, F. Electric Field Induced Structural Colour Tuning of a Silver/Titanium Dioxide Nanoparticle One-Dimensional Photonic Crystal. *Beilstein J. Nanotechnol.* **2016**, *7* (1), 1404–1410. https://doi.org/10.3762/bjnano.7.131.

(30) Anker, J. N.; Hall, W. P.; Lyandres, O.; Shah, N. C.; Zhao, J.; Van Duyne, R. P. Biosensing with Plasmonic Nanosensors. *Nature Materials*. 2008. https://doi.org/10.1038/nmat2162.

(31) Unser, S.; Bruzas, I.; He, J.; Sagle, L. Localized Surface Plasmon Resonance Biosensing: Current Challenges and Approaches. *Sensors (Switzerland)* **2015**, *15* (7), 15684–15716. https://doi.org/10.3390/s150715684.

(32) Chen, G.; Feng, Q. L.; Wu, J.; Chen, G. Q.; Cui, F. Z.; Kim, T. N.; Kim, J. O. A Mechanistic Study of the Antibacterial Effect of Silver Ions on Escherichia Coli and Staphylococcus Aureus. *J. Biomed. Mater. Res.* **2000**, *52* (4), 662–668. https://doi.org/10.1002/1097-4636(20001215)52.

(33) Ponja, S. D.; Sehmi, S. K.; Allan, E.; MacRobert, A. J.; Parkin, I. P.; Carmalt, C. J. Enhanced Bactericidal Activity of Silver Thin Films Deposited via Aerosol-Assisted Chemical Vapor Deposition. *ACS Appl. Mater. Interfaces* **2015**, *7* (51), 28616–28623. https://doi.org/10.1021/acsami.5b10171.

(34) Kim, J. S.; Kuk, E.; Yu, K. N.; Kim, J.-H.; Park, S. J.; Lee, H. J.; Kim, S. H.; Park, Y. K.; Park, Y. H.; Hwang, C.-Y.; et al. Antimicrobial Effects of Silver Nanoparticles.

Nanomedicine Nanotechnology, Biol. Med. **2007**, *3* (1), 95–101. https://doi.org/10.1016/j.nano.2006.12.001.

(35) Franci, G.; Falanga, A.; Galdiero, S.; Palomba, L.; Rai, M.; Morelli, G.; Galdiero, M. Silver Nanoparticles as Potential Antibacterial Agents. *Molecules* **2015**, *20* (5), 8856–8874. https://doi.org/10.3390/molecules20058856.

(36) Sondi, I.; Salopek-Sondi, B. Silver Nanoparticles as Antimicrobial Agent: A Case Study on E. Coli as a Model for Gram-Negative Bacteria. *J. Colloid Interface Sci.* **2004**, *275* (1), 177–182. https://doi.org/10.1016/j.jcis.2004.02.012.

(37) Dror-Ehre, A.; Mamane, H.; Belenkova, T.; Markovich, G.; Adin, A. Silver Nanoparticle–E. Coli Colloidal Interaction in Water and Effect on E. Coli Survival. *J. Colloid Interface Sci.* **2009**, *339* (2), 521–526. https://doi.org/10.1016/j.jcis.2009.07.052.

(38) Dakal, T. C.; Kumar, A.; Majumdar, R. S.; Yadav, V. Mechanistic Basis of Antimicrobial Actions of Silver Nanoparticles. *Front. Microbiol.* **2016**, *7* (NOV), 1–17. https://doi.org/10.3389/fmicb.2016.01831.

(39) Abbaszadegan, A.; Ghahramani, Y.; Gholami, A.; Hemmateenejad, B.; Dorostkar, S.; Nabavizadeh, M.; Sharghi, H. The Effect of Charge at the Surface of Silver Nanoparticles on Antimicrobial Activity against Gram-Positive and Gram-Negative Bacteria: A Preliminary Study. *J. Nanomater.* **2015**, *2015*, 1–8. https://doi.org/10.1155/2015/720654.

(40) El Badawy, A. M.; Silva, R. G.; Morris, B.; Scheckel, K. G.; Suidan, M. T.; Tolaymat, T. M. Surface Charge-Dependent Toxicity of Silver Nanoparticles. *Environ. Sci. Technol.* **2011**, *45* (1), 283–287. https://doi.org/10.1021/es1034188.

(41) Esteban-Ferrer, D.; Edwards, M. A.; Fumagalli, L.; Juárez, A.; Gomila, G. Electric Polarization Properties of Single Bacteria Measured with Electrostatic Force Microscopy. *ACS Nano* **2014**, *8* (10), 9843–9849. https://doi.org/10.1021/nn5041476.

(42) Müller, J.; Sönnichsen, C.; von Poschinger, H.; von Plessen, G.; Klar, T. A.; Feldmann, J. Electrically Controlled Light Scattering with Single Metal Nanoparticles. *Appl. Phys. Lett.* **2002**, *81* (1), 171–173. https://doi.org/10.1063/1.1491003.

(43) Kriegel, I.; Scotognella, F.; Manna, L. Plasmonic Doped Semiconductor Nanocrystals: Properties, Fabrication, Applications and Perspectives. *Phys. Rep.* **2017**, *674*, 1–52. https://doi.org/10.1016/j.physrep.2017.01.003.

(44) Scotognella, F.; Chiasera, A.; Criante, L.; Aluicio-Sarduy, E.; Varas, S.; Pelli, S.; Łukowiak, A.; Righini, G. C.; Ramponi, R.; Ferrari, M. Metal Oxide One Dimensional Photonic Crystals Made by RF Sputtering and Spin Coating. *Ceram. Int.* **2015**, *41* (7), 8655–8659. https://doi.org/10.1016/j.ceramint.2015.03.077.

(45) Malitson, I. H. Interspecimen Comparison of the Refractive Index of Fused Silica. *J. Opt. Soc. Am.* **1965**, *55* (10), 1205. https://doi.org/10.1364/JOSA.55.001205.

(46) Mendelsberg, R. J.; Garcia, G.; Li, H.; Manna, L.; Milliron, D. J. Understanding the Plasmon Resonance in Ensembles of Degenerately Doped Semiconductor Nanocrystals. *J. Phys. Chem. C* **2012**, *116* (22), 12226–12231. https://doi.org/10.1021/jp302732s.

(47) Garnett, J. C. M. Colours in Metal Glasses, in Metallic Films, and in Metallic Solutions. II. *Philos. Trans. R. Soc. A Math. Phys. Eng. Sci.* **2006**, *205* (387–401), 237–288. https://doi.org/10.1098/rsta.1906.0007.

(48) Bellingeri, M.; Chiasera, A.; Kriegel, I.; Scotognella, F. Optical Properties of Periodic, Quasi-Periodic, and Disordered One-Dimensional Photonic Structures. *Opt. Mater. (Amst).* **2017**, *72*, 403–421. https://doi.org/10.1016/j.optmat.2017.06.033.

(49) Born, M.; Wolf, E. *Principles of Optics: Electromagnetic Theory of Propagation, Interference*; 1999.

(50) Drude, P. Zur Elektronentheorie Der Metalle. *Ann. Phys.* **1902**, *312* (3), 687–692. https://doi.org/10.1002/andp.19023120312.

(51) Mock, J. J.; Smith, D. R.; Schultz, S. Local Refractive Index Dependence of Plasmon Resonance Spectra from Individual Nanoparticles. *Nano Lett.* **2003**, *3* (4), 485–491. https://doi.org/10.1021/nl0340475.

(52) Lotsch, B. V.; Knobbe, C. B.; Ozin, G. A. A Step Towards Optically Encoded Silver Release in 1D Photonic Crystals. *Small* **2009**, *5* (13), 1498–1503. https://doi.org/10.1002/smll.200801925.

(53) Kruijf, N. De; Beest, M. Van; Rijk, R.; Sipiläinen-Malm, T.; Losada, P. P.; Meulenaer, B. De. Active and Intelligent Packaging: Applications and Regulatory Aspects. *Food Addit. Contam.* **2002**, *19* (sup1), 144–162. https://doi.org/10.1080/02652030110072722.

(54) Lee, K. J.; Wu, J. W.; Kim, K. Enhanced Nonlinear Optical Effects Due to the Excitation of Optical Tamm Plasmon Polaritons in One-Dimensional Photonic Crystal Structures. *Opt. Express* **2013**, *21* (23), 28817. https://doi.org/10.1364/OE.21.028817.

(55) Symonds, C.; Azzini, S.; Lheureux, G.; Piednoir, A.; Benoit, J. M.; Lemaitre, A.; Senellart, P.; Bellessa, J. High Quality Factor Confined Tamm Modes. *Sci. Rep.* **2017**, *7* (1), 3859.

https://doi.org/10.1038/s41598-017-04227-1.

Supplementary information for

Hybrid 1D Plasmonic/Photonic Crystals for Optical Detection of Bacterial Contaminants

Giuseppe Maria Paternò[1†*], Liliana Moscardi[1,2†], Stefano Donini[1], Davide Ariodanti[3], Ilka Kriegel[4], Maurizio Zani[2], Emilio Parisini[1], [*] Francesco Scotognella[1,2] and Guglielmo Lanzani[1,2*]

[1]Center for Nano Science and Technology@PoliMi, Istituto Italiano di Tecnologia, Via Giovanni Pascoli, 70/3, 20133 Milano, Italy;

[2]Dipartimento di Fisica, Politecnico di Milano, Piazza Leonardo da Vinci 32, 20133 Milano, Italy.

[3]Dipartimento di Chimica, Materiali e Ingegneria Chimica "Giulio Natta", Piazza Leonardo da Vinci 32, 20133 Milano, Italy.

[4]Department of Nanochemistry, Istituto Italiano di Tecnologia (IIT), via Morego, 30, 16163 Genova, Italy

[†]These authors contributed equally to this work

[*] Corresponding authors

This file includes: Discussion on the biocidal activity of silver; scanning electron microscopy images of the silver film and cross-section of the 1D photonic crystal; UV-Vis absorption spectra of the silver films after dipping in liquid LB and *E. coli*/LB mixture; zone of inhibition in the agar plate inoculated with *E. coli*; UV-Vis transmission spectra of the Ag/BSs samples after dipping in liquid LB and *E. coli*/LB mixture; UV-Vis transmission spectra of the BSs without the silver layer before and after exposure to LB or to LB/*E. coli*.

Biocidal activity of silver

The antimicrobial properties of silver are well-known, and are exploited in a variety of everyday life applications[1,2].

For this reason, silver thin film and nanoparticles (NPs) have been employed in a range of applications as antibacterial agent, which can be also useful for addressing the problem of antibiotic resistance that is occurring in the last decade[3]. However, a unified and definitive explanation to describe this property has not been provided yet[4].

Various studies have related the cytotoxic effect of Ag to a combination of different reactions that take place within the prokaryotic cell[4]. Furthermore, it has been observed that the anti-bacterial efficacy depends on the type of bacteria[5]. The bacteria can be cataloged in Gram-positive and Gram-negative, based on the conformation of their membrane. In the former, the cell wall is composed of a thick layer of peptidoglycans, while the Gram-negatives have an outer membrane formed mainly by lipopolysaccharides and an inner one of peptidoglycans, much thinner than the previous ones[6]. Given the larger size of the Gram-positive cell wall, the endocytosis of the nanoparticles is more difficult, and therefore less effective for this kind of bacteria[3].

The cytotoxic effect of silver nanoparticles is more or less marked depending on concentration, shape, time and size[3,7,8]. NPs with dimensions smaller than 10 nm are more easily absorbed by endocytosis from the cell and interact with lysosomes and endosomes, in fact, thanks to their large specific surface area they are particularly reactive[3,7,9]. The acidic environment present inside the lysosomes favors chemical reactions that increase the presence of ROS (reactive oxygen species) and of superoxide anion (O^{2-}) produced by them, leading to an arise of oxidative stress. ROS cause an imbalance between the cell's ability to eliminate reactive intermediates and oxygen production[9]. Hydrogen peroxide (H_2O_2) contained in the ROS reacts with Ag NPs leading to the formation of

Ag ions: $2Ag + H_2O_2 + 2H^+ \rightarrow 2Ag^+ + 2H_2O$ [7]. Moreover, H_2O_2 can lead to the formation of ·OH, considered one of the most oxidative ROS, able to oxidize the whole cell. Nanoparticles and silver ions can escape from lysosomes, increasing intracellular ROS concentration[10]. Ag NPs and Ag ions reduce glutathione, thioredoxin, superoxide dismutase and thioredoxin peroxidase, as they react with thiol groups, contained in most of the cell including cytoplasm, mitochondria and cell membrane. Damage to the cell wall causes an increase in its permeability and a cytoplasm leak, thus leading to necrosis[11]. Also the lysosomal membrane rupture causes a lysosome-mediated apoptosis, pouring the cathepsins into the cytoplasm[11]. Ag NPs and Ag^+ cause damage to mitochondria by inhibiting the production of adenosine triphosphate (ATP), increasing oxidative stress, interfering with mitochondria impairs electron transfer, causing swelling and acceleration of mitochondrial respiration itself and leading to apoptosis[11,12]. Nuclear pore complex has an average diameter of 9-10 nm, hence small AgNPs can penetrate and deposit inside with a subsequent production of ROS that damages the DNA and generates chromosomal abnormalities[11]. Also Ag^+ has been seen to cause problems to DNA and induce apoptosis of the cells[7,10].

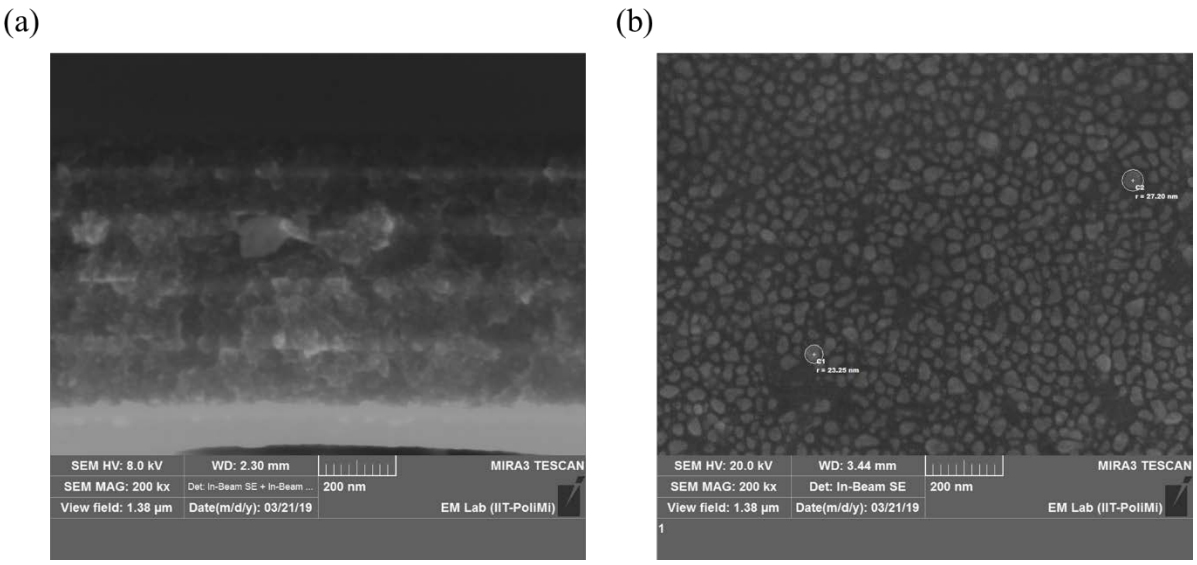

Figure S1 (a) Scanning electron microscopy (SEM) image of Ag/BS sample (cross section). (b) SEM of the Ag layer exhibiting the typical granular morphology.

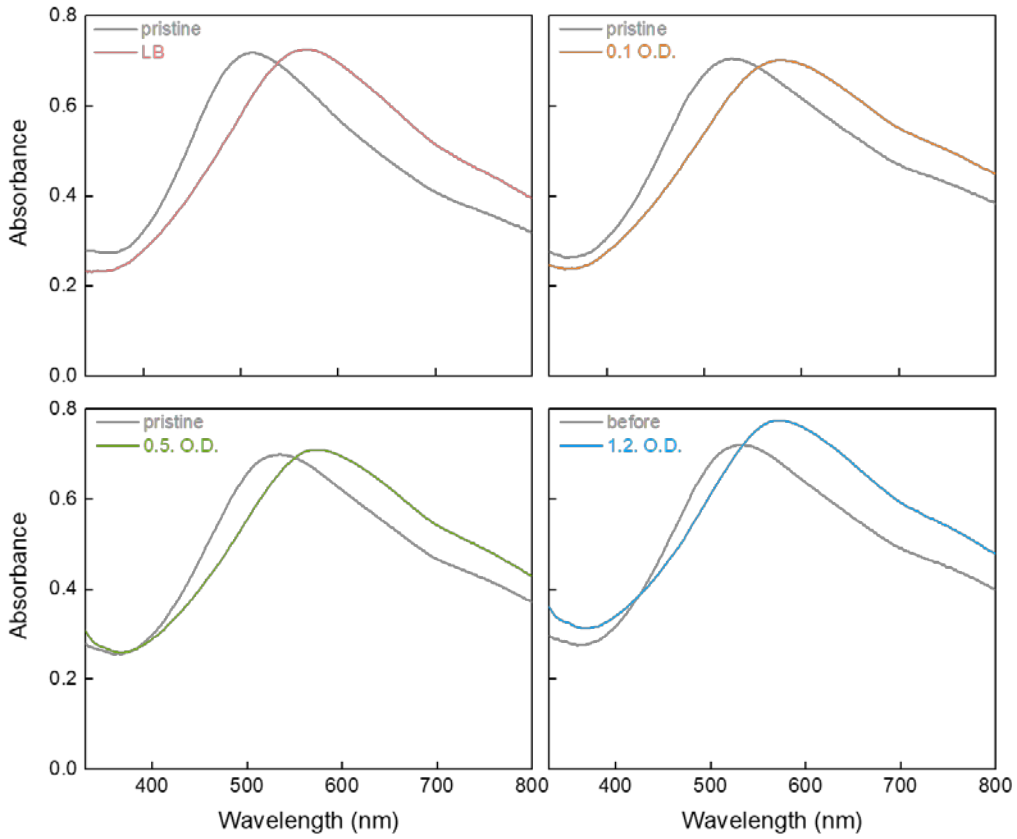

Figure S2. Optical absorption of a Ag thin film (8 nm on glass) before and after dipping in liquid LB or LB/*E. coli* mixture with increasing bacterial loading.

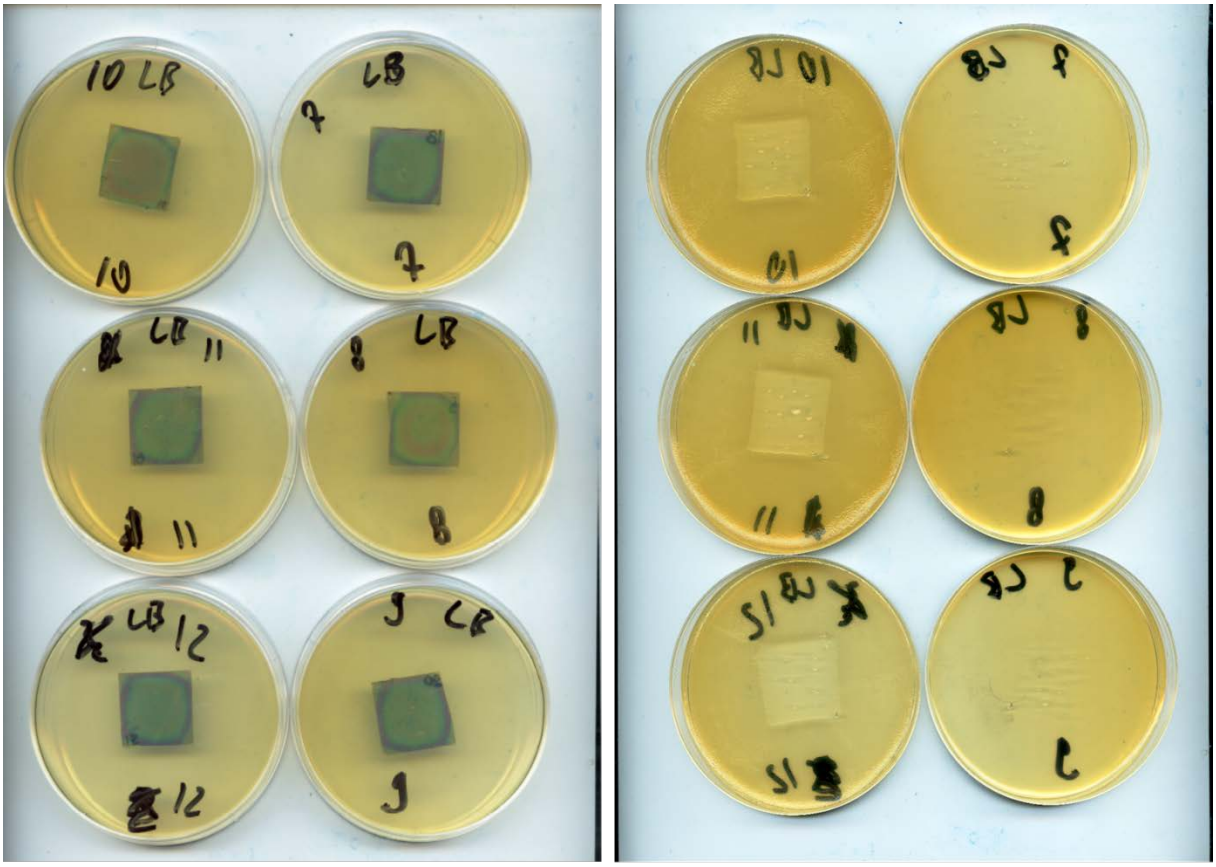

Figure S3. Picture of the Agar plate embedded with LB medium or inoculated with *E. coli* before (left) and after removal of our Ag/BSs.

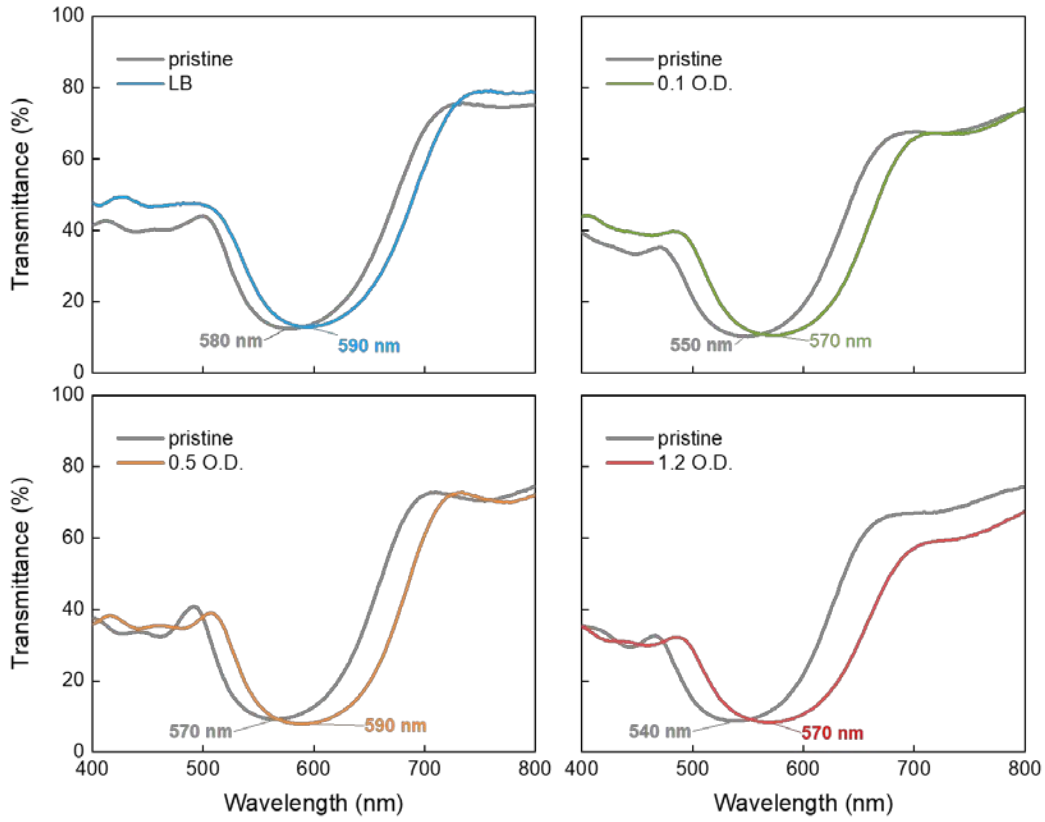

Figure S4. Transmission spectrum of the Ag/BSs before and after dipping in liquid LB or LB/E. coli mixture with increasing bacterial loading.

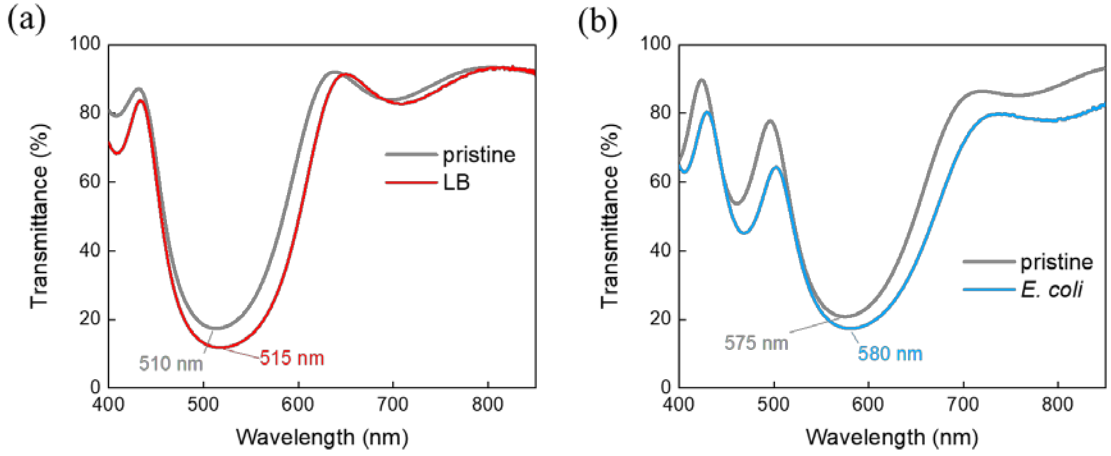

Figure S5. (a) Transmission spectrum of Ag/1D PhC after exposure to the LB medium (red-line) and (b) E. coli (blue-line) in agar plate.

1. Crabtree, J. H. *et al.* The efficacy of silver-ion implanted catheters in reducing peritoneal dialysis-related infections. *Perit. Dial. Int.* **23**, 368–74

2. Catauro, M., Raucci, M. G., de Gaetano, F. & Marotta, A. Antibacterial and bioactive silver-containing $Na_2O{\cdot}CaO{\cdot}2SiO_2$ glass prepared by sol–gel method. *J. Mater. Sci. Mater. Med.* **15**, 831–837 (2004).

3. Rai, M., Yadav, A. & Gade, A. Silver nanoparticles as a new generation of antimicrobials. *Biotechnol. Adv.* **27**, 76–83 (2009).

4. Franci, G. *et al.* Silver Nanoparticles as Potential Antibacterial Agents. *Molecules* **20**, 8856–8874 (2015).

5. Shrivastava, S. *et al.* Characterization of enhanced antibacterial effects of novel silver nanoparticles. *Nanotechnology* **18**, 225103 (2007).

6. Silhavy, T. J., Kahne, D. & Walker, S. The bacterial cell envelope. *Cold Spring Harb. Perspect. Biol.* **2**, a000414 (2010).

7. Wei, L. *et al.* Silver nanoparticles : synthesis , properties , and therapeutic applications. *Drug Discov. Today* **20**, 595–601 (2015).

8. Pal, S., Tak, Y. K. & Song, J. M. Does the antibacterial activity of silver nanoparticles depend on the shape of the nanoparticle? A study of the gram-negative bacterium Escherichia coli. *J. Biol. Chem.* **290**, 1712–1720 (2015).

9. Chang, Y.-N., Zhang, M., Xia, L., Zhang, J. & Xing, G. The Toxic Effects and Mechanisms of CuO and ZnO Nanoparticles. *Materials (Basel).* **5**, 2850–2871 (2012).

10. Guo, D. *et al.* Anti-leukemia activity of PVP-coated silver nanoparticles via generation of

reactive oxygen species and release of silver ions. *Biomaterials* **34**, 7884–7894 (2013).

11. Zhang, T., Wang, L., Chen, Q. & Chen, C. Cytotoxic potential of silver nanoparticles. *Yonsei Med. J.* **55**, 283–91 (2014).

12. Almofti, M. R., Ichikawa1, T., Yamashita3, K., Terada5, H. & Shinohara1, Y. Hayashi cho, Takamatsu 761-0395; 3School of Dentistry, The University of Tokushima 4Institute for Genome Research. *J. Biochem* **134**, 770–8503 (2003).